



ELSEVIER

Contents lists available at [SciVerse ScienceDirect](http://www.elsevier.com/locate/ijadhadh)

International Journal of Adhesion & Adhesives

journal homepage: www.elsevier.com/locate/ijadhadh

Influence of adhesive thickness on local interface fracture and overall strength of metallic adhesive bonding structures

Wei Xu*, Yueguang Wei

State Key Laboratory of Nonlinear Mechanics, Institute of Mechanics, Chinese Academy of Sciences, Beijing 100190, PR China

ARTICLE INFO

Article history:

Accepted 18 July 2012

Available online 7 August 2012

Keywords:

Finite element analysis

Cohesive zone model

Adhesive thickness

Metallic bonded joint

Overall strength

ABSTRACT

Adhesive bonding structures are widely used in a variety of engineering fields. Their overall strength is dependent on the cohesive properties involving local interface fracture. In the present research, the influence of the adhesive thickness on the cohesive properties and the overall strength of metallic adhesive bonding structures are investigated, with the cohesive zone model employed to equivalently simulate the adhesive layers with various thicknesses. A theoretical approach has been developed to determine the cohesive parameters for the present model when the adhesive thickness is varied. And then some numerical examples are given to explore the adhesive thickness-dependence overall strength of the adhesive joints, followed by some comparisons with the existing experimental results. Furthermore, the variations of both the cohesive parameters and the overall strength with the various thicknesses are influenced by some intrinsic characteristics of adhesives, which are investigated finally. The results show that both the cohesive parameters and the overall strength of metallic adhesive bonding structures are much dependent on the adhesive thickness, and the variations of overall strength resulting from the various thicknesses have discrepancy due to the toughness and strain hardening capacity of adhesives.

Crown Copyright © 2012 Published by Elsevier Ltd. All rights reserved.

1. Introduction

Adhesive bonding structures are economical, practical and easy to make and thus have been widely used to connect dissimilar materials in a variety of industries including civil engineering, automotive and aircraft industries. The strength evaluation and failure analysis of adhesively bonded joints in various applications are important topics. Accordingly, great efforts have been made in finding the influences of material and geometrical parameters on the load bearing capacity of adhesive bonding structures, so as to design optimal structures with proper adhesives for practical requirements in engineering.

Adhesive thickness is one of the most significant geometrical parameters, which attracts many researchers to study its effect on the overall strength of adhesive bonding structures. Recently, many experimental results have shown that the overall strength was influenced substantially by adhesive thickness. de Silva et al. [1,2] investigated the high strength steel single lap joints (SLJ) bonded by various types of epoxy adhesives layers. They found that load bearing capacity of the lap joints increased as the adhesive thickness was decreased. The similar results were pointed out by other researches that also concerned the effect of adhesive thickness on the overall strength for SLJ [3,4]. Furthermore, some other types of adhesively bonded joints have

also been studied experimentally. For example, Chai et al. [5] carried out the experimental research for adhesive thickness effect using the Napkin Ring specimen. They found that both the ultimate shear strength and strain increase monotonically with the decreasing adhesive thickness. Lee et al. [6] investigated the effect of adhesive thickness on the fracture toughness of compact tension adhesive-joint specimens, which showed the fracture toughness increased then tended to a stable value, with the increasing bond thickness. Similarly, tubular butt joint (TBJ) could be also regarded as a pure tensile specimen adopted by Castagnetti et al. [4] to study the influence of bond thickness, the result was found similar to the other tests mentioned above.

Although many experimental investigations have been implemented as mentioned above, the obtained results are still limited and local due to the experimental cost and complexity. In contrast, numerical modeling is considered to be an effective and useful approach to study the related issues of adhesive bonding. Accordingly, a variety of numerical models has been employed to attempt to explain the effect of adhesive thickness. Some researches modeled the adhesive layers using conventional elastic–plastic materials. The stress distributions could be hence obtained considering various adhesive thicknesses subjected to external loading. They claimed the thicker adhesive layer would cause higher interface stress, which therefore decreased the overall strength of adhesive bonding structures [2,7–9].

However, the overall strength of adhesive joints could not be obtained without considering the failure behavior of the adhesive layer. In other words, since the adhesive layers usually appear the

* Corresponding author. Tel.: +86 10 82543954; fax: +86 10 62561284.
E-mail address: xuwei@nm.imech.ac.cn (W. Xu).

elastic–plastic deformation behavior together with the cohesive damage and failure when subjected to external loading, the conventional elastic–plastic models are no longer applicable in modeling the failure process of adhesives. Alternatively, cohesive zone model (CZM) is a powerful approach to meet the above requirements. With this model, the adhesive layer is modeled as a cohesive surface with properties given by a traction–separation (T–S) law. The T–S law could be regarded as a representation of the constitutive properties of the adhesive layer [10]. Accordingly, the cohesive zone model of adhesive layer simulates the mechanical behavior of a material volume, not an atomic surface with greatly large separation strength (i.e., several GPa).

Both the separation strength and fracture energy are two sensitive cohesive parameters to describe the fracture properties of adhesives. Many researches in this area have been previously carried out in order to explore the influence of the adhesive thickness on the cohesive parameters, of which the fracture energy has been focused on by most groups [6,9,11–17]. Generally, as the adhesive thickness increases, the fracture energy (or critical energy release rate) increases to a peak value, and then either to keep stable [11,17], or gradually reduces to a plateau value corresponding to the bulk adhesive materials [9,15,16]. In contrast, the researches on the direct relationship between the separation strength and adhesive thickness are limited, which result from the following reason. Strictly speaking, the separation strength has been regarded as an intrinsic material parameter of an adhesive, which induces researchers to believe the separation strength would not vary when the adhesive thickness is varied. However, the CZM corresponding to an adhesive layer is used to simulate the mechanical behavior of a material volume, which could be seen as an equivalent method. The separation strength of the adhesive layer could be treated as an equivalent local strength and would be hence influenced by adhesive thickness, which has been confirmed by some previous experimental studies. Ji et al. [18–20] carried out a series of experiments to investigate the influence of adhesive thickness on the single mode and mixed-mode cohesive laws. It was observed that adhesive thickness had a substantial impact on both the fracture energy and the separation strength. Carlberger and Stigh [21] also implemented an experimental study to obtain the influence of adhesive thickness on cohesive properties of CZM, they also found the decrease in separation strength with the increasing adhesive thickness. Although some experimental and numerical analyses of the adhesive bonding structure with various adhesive thicknesses have been proposed by many researches, the understanding to the mechanisms of thickness-dependence cohesive properties has been still local. Besides, the underlying factors which affect the variation of the overall strength with the various thicknesses have been unclear yet.

In the present research, the influence of the adhesive thickness on both the cohesive parameters and the overall strength of metallic adhesively bonded joints are investigated, with the CZM employed to simulate the adhesive layers with a series of thicknesses. A theoretical approach has been developed to determine the CZM parameters for the present model when the adhesive thickness is varied. And then some numerical examples are shown to display the thickness-dependence overall strength of the adhesive joints, followed by some comparisons with the existing experimental results. Furthermore, the variations of the cohesive parameters and the overall strength with the various thicknesses are influenced by some intrinsic characteristics of adhesives, which are investigated finally.

2. Cohesive zone model

Cohesive zone models (CZMs) based on traction–separation (T–S) laws are well suitable to describe the de-cohesion behavior

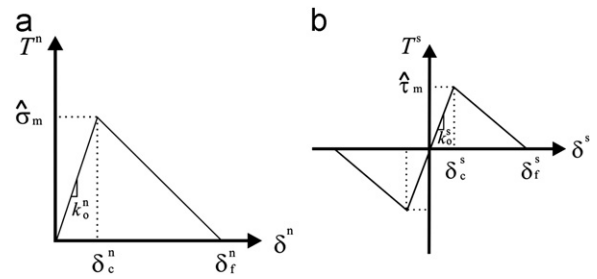


Fig. 1. Typical bilinear traction–separation law of cohesive zone model: (a) traction–separation relation in tension and (b) traction–separation relation in shear.

in composite structures. The CZMs require T–S relations for characterizing their constitutive laws. So far, considerable researches have focused on the constitutive laws of CZMs and their applications [22]. It has been established that whilst the peak value and area of the T–S curve are vital for capturing the interface separation behavior, its precise shape is of less significance. Consequently, for simplicity, the bilinear T–S law shown in Fig. 1 is selected for the present study [22,23]. Built upon the bilinear cohesive zone model (CZM), the adhesive layer could be treated as interface between the two metallic adherends, is modeled with the cohesive zone elements.

Fig. 1 shows the T–S relation of the CZM, with Fig. 1a and b giving the relationships in normal and shear directions, respectively. To distinguish the normal T–S law from the shear one, the superscript “n” represents the normal direction and “s” denotes the shear direction. In Fig. 1, δ_c and δ_f are the critical and failure separation displacements, respectively, and T is the traction stress.

Since the maximum value of T^n is $\hat{\sigma}_m$ while that of $|T^s|$ is $\hat{\tau}_m$, the interface fracture energy in the two directions can be expressed as

$$\Gamma^n = \int_0^{\delta_f^n} T^n d\delta^n = \frac{1}{2}\hat{\sigma}_m\delta_f^n$$

$$\Gamma^s = \int_0^{\delta_f^s} T^s d\delta^s = \frac{1}{2}\hat{\tau}_m\delta_f^s \quad (1)$$

As the loading is increased beyond a critical value, the interface begins to soften, and degrade, namely, the interface is now in the damaged (or softening) state. Typically, damage is initiated when a certain criterion is satisfied. In the present study, inspired by the bilinear law of Fig. 1, the quadratic nominal stress criterion is adopted to characterize interfacial damage, described as

$$\left(\frac{\langle T^n \rangle}{\hat{\sigma}_m}\right)^2 + \left(\frac{T^s}{\hat{\tau}_m}\right)^2 = 1 \quad (2)$$

where $\langle \cdot \rangle$ represents the Macaulay bracket defined by $\langle x \rangle = (x + |x|)/2$, with the usual interpretation that a pure compressive deformation or stress state does not initiate damage. The peak traction stresses $\hat{\sigma}_m$ and $\hat{\tau}_m$ are termed the normal and shear separation strengths, respectively.

It is assumed that interfacial damage occurs when Eq. (2) is satisfied and a single damage variable D based on the total displacement jump Δ is introduced (i.e., $\Delta = \sqrt{\langle \delta^n \rangle^2 + (\delta^s)^2}$) [24,25] as

$$D = \frac{\Delta_f(\Delta_{\max} - \Delta_c)}{\Delta_{\max}(\Delta_f - \Delta_c)} \quad (3)$$

where Δ_c and Δ_f denote the total displacement at damage initiation and complete failure. The quantity, Δ_f is determined by $\Delta_f = 2I_c^{\text{mixed}}/T_c^{\text{eff}}$ with T_c^{eff} denoting the effective traction at damage initiation (i.e., $T_c^{\text{eff}} = \sqrt{(T_c^n)^2 + (T_c^s)^2}$). In Eq.(3), Δ_{\max}

denotes the maximum total displacement experienced during the loading history.

Γ^{mixed} is the mixed total fracture energy of the adhesive. Generally, Γ^{mixed} depends on the mode-mixity. In other words, Γ^{mixed} varies as a function of the mode-mixity. In the present investigation, Γ^{mixed} is determined by the linear fracture criterion, which can be expressed as

$$\frac{G^n}{\Gamma^n} + \frac{G^s}{\Gamma^s} = 1 \tag{4}$$

where G^n and G^s denote work done by the traction and its conjugate relative displacement in the normal and shear directions, respectively. Γ^n and Γ^s refer to the total energy required to cause failure in the pure normal and shear directions, respectively, as defined in Eq. (1). Consequently, Γ^{mixed} can be obtained by

$$\Gamma^{\text{mixed}} = G^n + G^s \tag{5}$$

when Eq. (4) is satisfied.

3. Thickness-dependence cohesive parameters

When the cohesive zone model is employed to simulate the adhesive layer, the progressive failure of the adhesive could be captured by the aforementioned bilinear traction–separation law, which is defined by three cohesive parameters, namely, initial stiffness, total fracture energy and separation strength [26]. All of these parameters would be influenced by the adhesive thickness. In this section, the relationship between these parameters and thickness would be presented as follows.

3.1. Initial stiffness

The initial stiffness of CZ model represents the slope value of the rising part of the T–S curve shown in Fig. 1. It is used to describe the ratio between the cohesive stress and separation displacement before the adhesive damage occurs, which is similar to the stiffness coefficient of a spring. Obviously, the initial stiffness is dominated by the elastic properties together with the adhesive thickness t . In the present investigation, following the way in the previous researches [27,28], initial stiffness could be expressed as

$$k_0^n = \frac{E}{t} \quad \text{and} \quad k_0^s = \frac{G}{t} \tag{6}$$

where E and G denote the Young’s modulus and shear modulus, respectively. Linked with the initial stiffness, the relation between the separation strength $\hat{\sigma}$ and critical separation displacement k_0 could be obtained

$$\delta_c = \frac{\hat{\sigma}}{k_0} \tag{7}$$

Note that the superscripts denoting the normal and shear directions (i.e., n and s) are omitted for simplicity, followed by the equations below.

3.2. Total fracture energy

Generally, the mixed total fracture energy of CZM could be determined by Eq. (5) when considering the adhesive layer as an equivalent cohesive layer. In other aspect, the adhesive layer with a certain thickness would dissipate two types of energies, including the cohesive energy Γ_0 and plastic dissipation energy Γ_p , which denote the energy making the adhesive layer separated and the energy dissipated during the plastic deformation, respectively. Γ_0 could be regarded as intrinsic work of fracture associated with

the embedded cohesive zone and Γ_p could be regarded as the contribution to the bond toughness arising from the plastic dissipation and stored elastic energy within the adhesive layer [11]. Accordingly, the total fracture energy Γ can be expressed below

$$\Gamma = \Gamma_0 + \Gamma_p \tag{8}$$

where Γ_p can be obtained by integrating the work density far downstream along the adhesive layer thickness [11], which is

$$\Gamma_p = \int_0^t \left(\int_0^{\varepsilon_{ij}^D} \sigma_{ij} d\varepsilon_{ij} \right) dy \tag{9}$$

where ε_{ij}^D is the strain component at the downstream adhesive layer, integration “dy” is along the thickness of the adhesive layer. The previously similar work [11,29] has pointed out a full damage process would take place in the adhesive layer when the adhesive thickness is not too thick, and Γ_p can be estimated approximately by

$$\Gamma_p \approx tU \tag{10}$$

where U is the area below the stress–strain curve of the adhesive material, also could be seen as the mean plastic work per unit adhesive volume.

It should be noted that Eq. (10) is applicable only under the specific condition, which indicates the adhesive thickness is smaller than plastic zone height in front of crack tip. In fact, the plastic dissipation Γ_p is significantly influenced by the plastic zone height that would be constrained by the adhesive thickness [6,11,14,15].

In the present study, the crack plane is assumed in the middle of adhesive layer. The length that scales the plastic dissipation zone in front of crack tip, for the plane strain small-scale yielding (SSY) condition, is expressed as [11]

$$r_p(\theta) = \alpha(\theta) \frac{1}{3\pi} \frac{E}{1-\nu^2} \frac{\Gamma_0}{\sigma_s^2} \tag{11}$$

where θ is the angle defined with respect to the crack plane. The plastic zone height is evaluated corresponding to $\theta = 90^\circ$, which is usually larger than $r_p(\theta)$ with other values of θ . Thus $r_p(90^\circ)$ could be regarded as equal to r_p^{max} . Typically, $\alpha(90^\circ)$ ranges between 1.25 and 5 according to Pardoen et al. [11], and 1.25 is selected in the present investigation. Furthermore, it should be pointed out that Eq. (11) is obtained under the SSY condition, which means the adherends are materials with either thick size or high elastic modulus. If the conditions of adherends are not met, namely, the adherends are thin materials with a low elastic modulus, with the increasing adhesive thickness, the plastic zone height increases to a maximum value and then decreases to reach the SSY condition value depicted by Eq. (11) and keeps steady. In other words, the maximum value may be remarkably larger than the SSY condition value. By contrast, when the SSY conditions are met, the maximum value appears approximately equal to the SSY condition value [11], which is considered in the present investigation for simplification. In short, when the adhesive thickness is smaller than the plastic zone height, the plastic dissipation energy part would be obtained by Eq. (10), and when the adhesive thickness is larger than the plastic zone height, the plastic dissipation energy would maintain at a constant value that is dominated by r_p^{max} . Based on the above statement, the total fracture energy would be expressed by

$$\Gamma = \Gamma_0 + \Gamma_p = \Gamma_0 + \int_0^t \left(\int_0^{\varepsilon_{ij}^D} \sigma_{ij} d\varepsilon_{ij} \right) dy = \begin{cases} \Gamma_0 + Ut & (t < 2r_p^{\text{max}}) \\ \Gamma_0 + 2Ur_p^{\text{max}} & (t \geq 2r_p^{\text{max}}) \end{cases} \tag{12}$$

3.3. Separation strength

As mentioned above, the separation strength refers to the peak traction stress in the T–S curve describing the CZM. When a crack

extends in an adhesive layer, the separation strength is usually used to characterize the largest cohesive stress between the upper and lower crack plane in front of crack tip. Thus, some previous researchers believed the separation strength was an intrinsic material parameter and would maintain constant for various adhesive thicknesses [11]. However, the situation would be somewhat different when the CZM is utilized in adhesive bonding structures. Instead of characterizing the cohesive stress in front of crack tip embedded within continuum adhesive materials, the CZM is employed to equivalently characterize the cohesive relation between the upper and lower adherends. The aforementioned crack is actually created due to the failed and disappeared CZ elements. And the separation strength is therefore substantially affected by various adhesive thicknesses, which is confirmed by numerous previous researches [18–21].

As mentioned above, δ_c and δ_f are the critical and maximum separation displacements, respectively. Therefore, the ratio between these separation displacements is introduced and named as the critical separation ratio λ , shown below

$$\lambda = \frac{\delta_c}{\delta_f} \tag{13}$$

When the adhesive thickness is varied, it is obvious that both the critical and maximum separation displacements change simultaneously due to the external constraint. In other words, with the increasing adhesive thickness, both of the two separation displacements would increase. Furthermore, the previous experimental investigations on the CZM influenced by adhesive thickness have shown the critical separation ratio δ_c/δ_f seems approximately unchanged [18–20]. Based on these considerations, the present investigation supposes the critical separation ratio λ is independent of adhesive thickness. In other words, λ would be unchangeable with the various thicknesses for a given type of adhesive. In additions, since the cohesive law in the normal direction usually appears different from that in shear direction, λ in the two directions are generally not identical.

Inspired by the bilinear law of Fig. 1, the separation strength could be obtained by

$$\hat{\sigma} = \frac{2\Gamma}{\delta_f} \tag{14}$$

Combining Eqs. (7), (13) and (14)

$$\hat{\sigma} = \frac{2\Gamma}{\delta_c/\lambda} = \frac{2\lambda\Gamma}{\delta/k_0} \tag{15}$$

and the separation strength could be hence rewritten

$$\hat{\sigma} = \sqrt{2\lambda k_0 \Gamma} \tag{16}$$

When CZM is used for simulating the adhesive layer with a comparatively smaller thickness, the separation strength usually appears larger than bulk fracture strength of the adhesive. However, the separation strength would be identical to the bulk fracture strength σ_f when the adhesive thickness increases to a certain critical value, which has been pointed out by numerous experimental observations [2,5,18–20]. In the present study, the critical value of adhesive thickness is termed critical thickness and denoted by t_c and the corresponding initial stiffness is k_{0c} . Thus λ could be rewritten by combining Eqs. (7), (12), (13) and (14)

$$\lambda = \frac{\delta_c}{\delta_f} = \frac{(\sigma_f/k_{0c})}{(2(\Gamma_0 + Ut_c)/\sigma_f)} = \frac{(\sigma_f)^2}{2k_{0c}(\Gamma_0 + Ut_c)} \tag{17}$$

substitution of Eq. (17) into Eq. (16) results in

$$\frac{\hat{\sigma}}{\sigma_f} = \sqrt{\frac{k_0\Gamma}{k_{0c}(\Gamma_0 + Ut_c)}} = \sqrt{\left(1 + \frac{Ut_c}{\Gamma_0}\right) \cdot \left(\frac{t}{t_c}\right)} \tag{18}$$

In the present study, a dimensionless parameter η is introduced based on intrinsic energy parameters, namely, $\eta = Ut_c/\Gamma_0$. Accordingly, substitution of Eq. (12) into Eq. (18) leads

$$\frac{\hat{\sigma}}{\sigma_f} = \begin{cases} \sqrt{\frac{1 + \eta\left(\frac{t}{t_c}\right)}{(1 + \eta)\left(\frac{t}{t_c}\right)}} & (t < 2r_p^{\max}) \\ \sqrt{\frac{2Ur_p^{\max}}{1 + \frac{\Gamma_0}{t_0}}} & (t \geq 2r_p^{\max}) \end{cases} \tag{19}$$

Eq. (19) presents the expression of the separation strength, which is given considering two cases with respect to two adhesive thickness ranges, respectively. Especially, when the adhesive thickness is larger than the plastic zone height, the separation strength would maintain at a constant as the adhesive continues to increase. It can be conjectured that the constant should be equal to 1, which means the separation strength is identical to the bulk fracture strength. Based on the above analysis, it can be deduced that the relation $t_c = 2r_p^{\max}$, and Eq. (19) could be hence rewritten as

$$\frac{\hat{\sigma}}{\sigma_f} = \begin{cases} \sqrt{\frac{1 + \eta\left(\frac{t}{t_c}\right)}{(1 + \eta)\left(\frac{t}{t_c}\right)}} & (t < t_c) \\ 1 & (t \geq t_c) \end{cases} \tag{20}$$

Furthermore, benefiting from introducing the dimensionless parameter η and the relation of $t_c = 2r_p^{\max}$, Eq. (12) could be simplified into dimensionless form

$$\frac{\Gamma}{\Gamma_0} = \begin{cases} 1 + \eta\left(\frac{t}{t_c}\right) & (t < t_c) \\ 1 + \eta & (t \geq t_c) \end{cases} \tag{21}$$

It can be found in Eqs. (20) and (21) that η is a very important parameter, which controls both the total fracture energy and the separation strength. Noting r_p^{\max} is expressed by Eq. (11), η could be given as follows, considering the relation of $t_c = 2r_p^{\max}$

$$\eta = \alpha(90^\circ) \frac{2}{3\pi} \frac{UE}{\sigma_s^2(1 - \nu^2)} \tag{22}$$

which indicates that η is independent of the intrinsic cohesive fracture energy Γ_0 . Moreover, by introducing the parameters η together with the relation of $t_c = 2r_p^{\max}$, λ in Eq. (17) could be rewritten below

$$\lambda = \frac{\alpha(90^\circ)}{3\pi(1 + \eta)(1 - \nu^2)} \left(\frac{\sigma_f}{\sigma_s}\right)^2 \tag{23}$$

It can be seen that λ is related to η . In particular, λ could be further simplified to the form of Eq. (24) when σ_f is treated equal to σ_s

$$\lambda = \frac{\alpha(90^\circ)}{3\pi(1 + \eta)(1 - \nu^2)} \tag{24}$$

It can be known from Eqs. (23) and (24) that λ increases with the decreasing η , which can be understood by the physical interpretation of η . In details, η could be employed to assess the toughness of adhesives layer, which is larger for a larger η . It is implied in Fig. 1 that the softening stage would be large for a smaller λ , which means relatively larger energy dissipation in the soften stage of adhesives.

In order to clearly present the variation of the cohesive parameters with the various thicknesses, Fig. 2a and b depicts the dimensionless separation strength and total fracture energy plotted as a function of the normalized adhesive thickness, respectively, according to Eqs. (20) and (21). The results of Fig. 2 demonstrate that the adhesive thickness and η have a

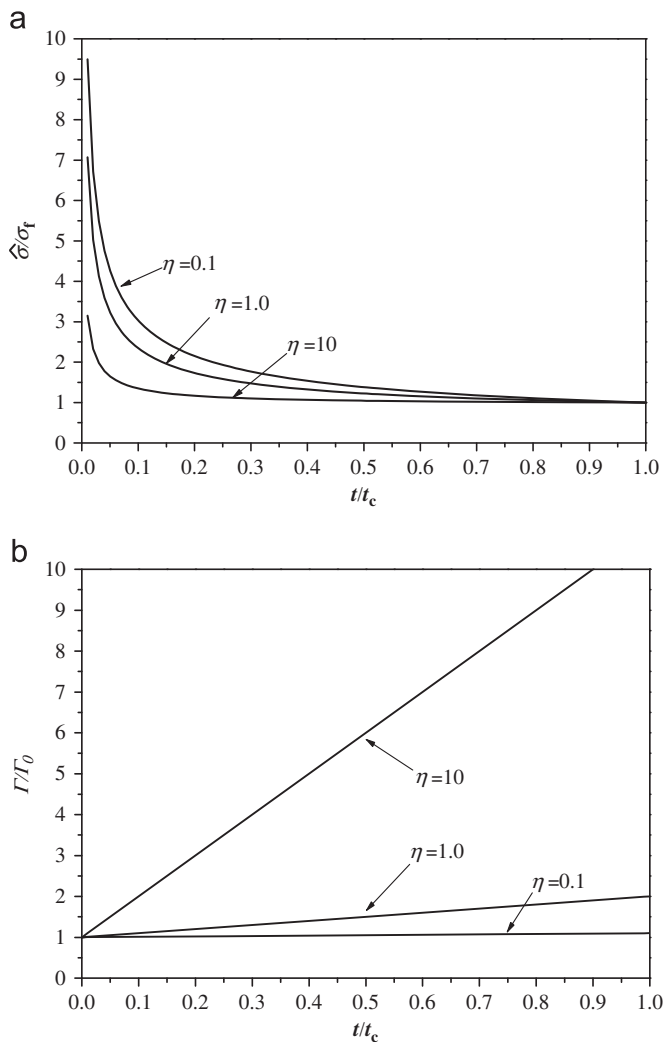


Fig. 2. (a) Normalized separation strength and (b) total fracture energy plotted as functions of adhesive thicknesses for selected toughness ratios η .

combined effect on the cohesive parameters. In details, as the adhesive thickness is decreased, the separation strength increased sharply for a small η (e.g., $\eta=0.1$), while the separation strength increased slowly for a relatively large η (e.g., $\eta=10$). It is worth noting that all the separation strength curves rise remarkably when the thickness approaches to 0. Furthermore, the rise gradient (i.e., slope of the curves) of the separation strength is larger for a smaller η . By contrast, the total fracture energy decreases as the thickness is decreased and the decrease gradient is larger for a larger η . It should be pointed out that the separation strength would increase up to more than seven times bulk fracture strength as shown in Fig. 2a, which is physically realistic with consideration of application for strain gradient plastic theory [30,31]. Nevertheless, molecular level calculations and further measurements are still needed to assess whether the potential separation strengths for adhesive layers have fundamental validity.

4. Numerical results and discussion

With the CZM and its thickness-dependence cohesive parameters presented above, the influence of the adhesive thickness on the overall mechanical behaviors of an adhesively bonded joint could be obtained. In this section, a numerical model of the joint

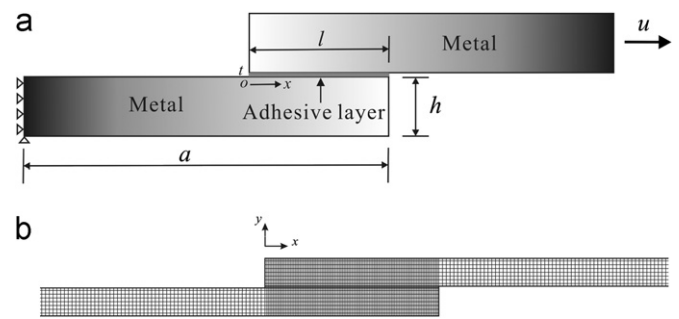


Fig. 3. (a) Numerical model of single lap joint (SLJ) for validating the present thickness-dependence cohesive parameters and (b) its finite element mesh.

lap joint (SLJ) is built with the commercially available FEM code ABAQUS. For the present model, since the width of the adherends used for the joint is far larger than the thickness, the joints under tension can be treated as an elastic–plastic plane strain problem.

4.1. Model validation

Fig. 3a depicts the computational model of the SLJ, which consists of two similar metallic adherends of thickness of h , having a typical value of 2 mm. The length of the adherends a is assigned the value of 120 mm. The adherends are connected by the adhesive layer of length l , which is also called the overlap length, assigned the value of 25 mm. The adherends are meshed using four-node quadrilateral plane strain elements. Under uniaxial stretching, the joint is deformed under plane strain. In the numerical models, the left side of the joint is fixed in the horizontal direction and the lower left corner is also fixed in the vertical direction. The model is loaded by means of an increasing displacement and a uniform displacement of u is applied to the right side of the joint.

The metallic adherends are modeled as elastic–plastic solids, with their true stress–strain curves fitted using power-law hardening laws [11,32] as

$$\sigma = \begin{cases} E\varepsilon & \varepsilon \leq \sigma_s/E \\ \sigma_s \left(\frac{\varepsilon}{\sigma_s/E} \right)^N & \varepsilon > \sigma_s/E \end{cases} \quad (25)$$

where E is the Young's modulus, N is the strain hardening exponent, and σ_s is the yield strength. For the present model, the metallic adherends are assumed to be the high strength steel with these three material properties having the values of 200 GPa, 0.078 and 400 MPa, respectively.

The adhesive layer is modeled with a single layer of four-node cohesive elements, which shares nodes with the neighboring elements in the upper and lower metallic adherends. In order to obtain better computational accuracy, the overlap region is densely meshed while sparse mesh is adopted in other regions as shown in Fig. 3b.

The characteristics of the cohesive elements applied in modeling the adhesive layer have been presented in Sections 2 and 3. For a purpose of validating the present theoretical approach for the thickness-dependence cohesive parameters, the overall mechanical response of the SLJ is calculated. In this section, two different types of adhesives are considered: one is a very ductile adhesive (i.e., Hysol EA 9361, Loctite), and the other is a comparatively brittle adhesive (i.e., Hysol EA 9321, Loctite), with the material properties taken from the previous literature [2] and shown in Table 1. Based on the approach proposed in Section 3.3, the toughness ratio η could be hence obtained, with the ductile and the brittle adhesives having the values of 31.8 and 2.8, respectively.

Table 1
Material parameters for two types of adhesives [2].

Parameters	Hysol EA 9321	Hysol EA 9361
Young's modulus E (GPa)	3.87	0.67
Poisson's ratio ν	0.36	0.4
Yield strength σ_s (MPa)	21.99	4.23
Tensile strength σ_f (MPa)	45.97	7.99
Toughness U (MPa)	1.16	2.69
Γ_0^n (N mm ⁻¹)	0.45	2.61
Γ_0^s (N mm ⁻¹)	0.90	5.22

The calculation is carried out in two steps, which involve the determination of the cohesive parameters and achieving the mechanical response under external loading. For the first step, the three thickness-dependence important cohesive parameters, namely, the initial stiffness, total fracture energy and separation strength, have been obtained according to the theoretical approach mentioned in Section 3. In order to show the direct relations between the cohesive laws and the various adhesive thicknesses, the T–S curves of these two types of adhesives for the selected thicknesses are plotted together in Fig. 4. Since the cohesive properties in shear direction are different from those in normal direction, the T–S curves in the two directions are hence different, which are separately presented in Fig. 4. It can be observed that the adhesive thickness has a significant influence on the T–S curves. With the decreasing of the adhesive thickness, the peak values of the T–S curves increase gradually, accompanied with the decreasing areas of the curves. The fundamental tendency of the present obtained T–S curves keep consistent with the previous experimental results [20].

By employing the above obtained cohesive parameters for the present model, the overall mechanical behavior of the SLJ model could be gained. The typical load–displacement curves for the two types of adhesives are shown in Appendix: A1, considering the adhesive thickness of 1.0 mm. It should be pointed out the obtained load refers to the force per unit width of the joint since the plane strain model is adopted. Note that the loads increase to peak loads and then decline with the increasing displacements. Although the peak loads correspond neither to crack initiation nor to the onset of instability [33], it has been widely accepted that the overall strength or the load-carrying capacity of SLJ could be assessed by the peak value of the load–displacement curve, which is usually called peak load [2,3,34,35]. In the present investigation, the variations of the peak loads for various adhesive thicknesses are therefore concerned.

In order to clearly show the influence of adhesive thickness on the overall strength of the joints, as presented in Fig. 5, the peak load F_p is plotted as a function of the various thicknesses for the two types of adhesives. It should be noted that the selected adhesive thicknesses are varied within the range of the interval [0.2, 1.0] mm, for a purpose of comparing with the corresponding experimental study which considers the same thickness range [2]. By the theoretical approach aforementioned in Section 3, the cases for other values of adhesive thicknesses could be also obtained if necessary. The calculated results depicted in Fig. 5 demonstrate the overall strength of the adhesive bonding structures decreases with the increasing adhesive thickness. For a purpose of checking the feasibility of the present numerical method, the existing experimental results [2] with the adoption of the same adhesives are compared with the present computational predictions. Overall, the present calculated results agree well with those measured. Noting that both the measured and the calculated results depicted in Fig. 5 are original data without any dimensionless processing, thus it can be judged that the accuracy of the present calculated methods is satisfactory and the present

theoretical approach considering the thickness-dependence cohesive law is convincing.

4.2. Effect of toughness ratio η

Based on the above calculations, the overall strength of adhesive bonding structures would increase as the adhesive thickness is gradually decreased. The increase tendency of the overall strength would be influenced by some important factors, which are discussed in the following sections.

As described in the aforementioned text, the toughness ratio η is a significant parameter because both the separation strength and the total fracture energy are related to it, which is indicated by Eqs. (20) and (21). η is also an intrinsic material parameter independent of the adhesive thickness. It can be found in Eq. (24) that η has relationship with another intrinsic material parameter λ . Furthermore, as described in Section 3.3, both of the two dimensionless parameters could be utilized to assess the toughness of materials. Thus it is adequate to only explore the effect of η . In this section, σ_f is treated equal to σ_s for simplification and Eq. (24) is therefore applicable.

For a purpose of making the present results representative, both the peak load and the adhesive thickness are normalized. Note that the adhesive thickness in practice may be larger than the critical thickness t_c , beyond which variation of the overall strength can be ignored. Thus the adhesive thicknesses are considered within the range smaller than t_c (i.e., $t \leq t_c$).

Fig. 6 plots the normalized peak load as a function of the normalized adhesive thickness for some selected values of η , namely, 0.1, 1.0 and 10, which represent a very brittle, an intermediate and a very ductile adhesives, respectively. The original experimental results are presented by discrete data points, which can be fitted by continuous and smooth curves having the expression of exponential form, namely, Eq. (26), with the values of fitting parameters (i.e., A_1 , A_2 , and A_3) given in Table 2.

$$\frac{F_p}{\sigma_f t} = A_1 e^{-\left(\frac{t/t_c}{A_2}\right)} + A_3 \quad (26)$$

The results of Fig. 6 demonstrate that the toughness ratio η has a significant effect on the load bearing capacity of the adhesive bonding structure. Although the peak load declines with the increasing thickness, it is observed that the decline styles corresponding to the three toughness ratios η have remarkable discrepancy. In details, for the case of $\eta = 0.1$, the curve declines sharply from the beginning to the end. Though the curve for $\eta = 1.0$ appears that the tendency of the decline is remarkable as well, obviously, the decline gradient can be easily found having discrepancy as the thickness is varied. By contrast, the curve for $\eta = 10$ shows a completely different style, which exhibits declines at first stage followed the nearly horizontal stage.

In order to further present the variation of decline tendencies for the three curves, Fig. 7 is plotted to show the absolute values of tangential slope along the each curves, denoted by κ , which is derived from Eq. (26) and shown below

$$\kappa = \left(\frac{A_1}{A_2}\right) e^{-\left(\frac{t/t_c}{A_2}\right)} \quad (27)$$

It is seen in Fig. 7 that the curves for the three values of η appear distinctly different. The curve for the small η (i.e., $\eta = 0.1$) exhibits relatively straight, while the curve for the large η (i.e., $\eta = 10$) exhibits relatively flexural. In other words, the change rate of κ is larger for the larger η .

The influence of the toughness ratio η could be understood in the view of the competition between the separation strength and

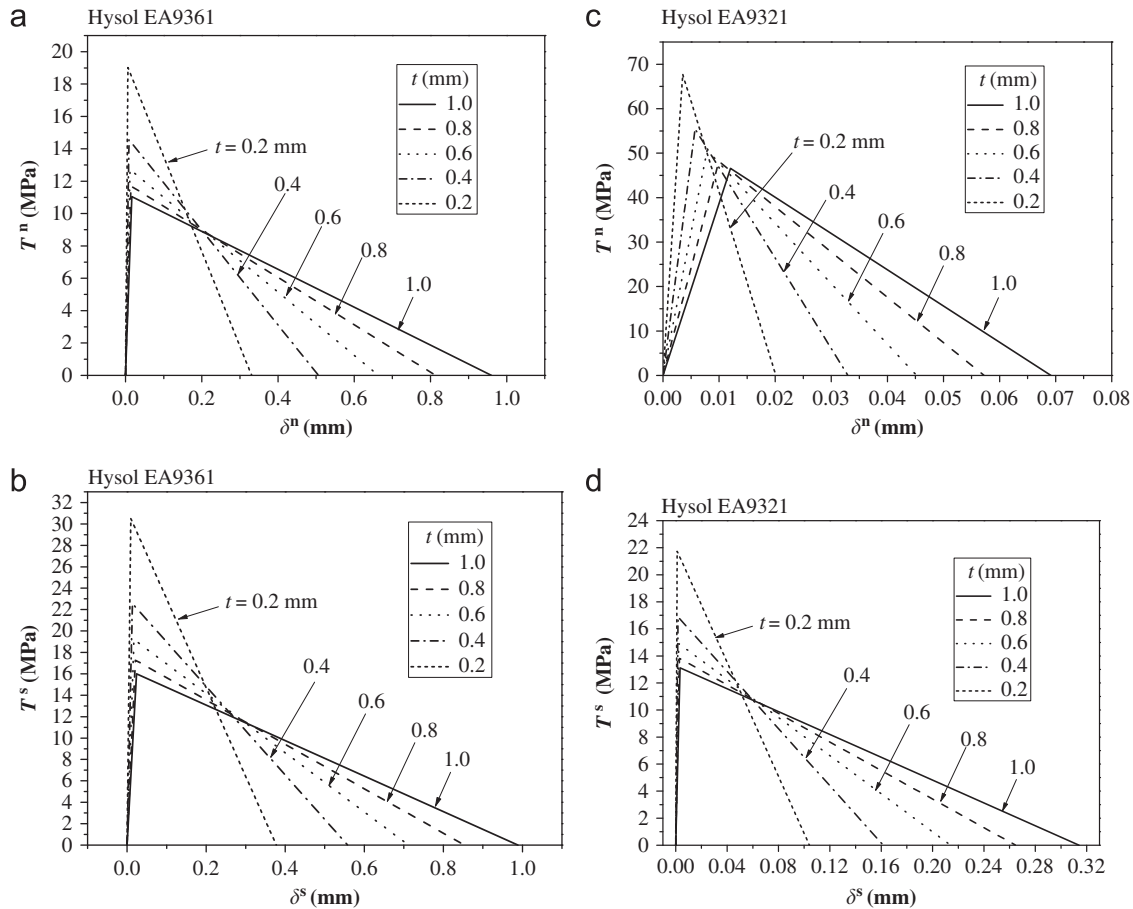


Fig. 4. Influence of various thicknesses on the obtained cohesive laws of adhesives in two directions: (a) Hysol EA 9361 in tension, (b) Hysol EA 9361 in shear, (c) Hysol EA 9321 in tension, and (d) Hysol EA 9321 in shear.

total fracture energy. As presented in Fig. 2, η has a substantial influence on the variations of both the separation strength and total fracture energy with the increasing thickness. However, the separation strength is increased while the total fracture energy is yet decreased. Previous study has pointed out that increasing the two cohesive parameters could improve the overall strength of adhesive bonding structures [36], but the two cohesive parameters in the present study are varied oppositely with the decreasing thickness. Thus the variation of the overall strength is controlled by the parameter playing a leading role. When η is relatively small (i.e., $\eta = 0.1$), with the decreasing thickness, the increase of separation strength is very noticeable while the decrease of the total fracture energy is slight, consequently, the overall strength appears the remarkable rising tendency. In other aspect, when η is relatively large (i.e., $\eta = 10$), with the decreasing thickness, the increase of separation strength is slight, especially in the range of thickness approaching to t_c , the overall strength appears the slight rising tendency even if the fracture energy seems increasing evidently. Based on the above discussion, it can be conjectured that the separation strength plays a principal role compared to the total fracture energy, which has been also confirmed by some previous investigations [1,35,36].

4.3. Effect of strength ratio σ_f/σ_s

It can be seen in Eq. (23) that the ratio between the failure strength and yield strength σ_f/σ_s is another key parameter. In fact, the ratio is also an intrinsic material parameter, which could be utilized to assess the strain hardening capacity of adhesive. It is

implied that the strain hardening capacity is improved as the strength ratio is increased.

In this section, the influence of σ_f/σ_s on the relationship between the peak load and the adhesive thickness is considered, which is depicted in Fig. 8. In order to simultaneously show the discrepancy resulting from η , two typical values of η (i.e., 1.0 and 10) are considered and shown in Fig. 8a and b, respectively. Both of the two figures have taken three strength ratios into account, namely, 1.0, 1.5, and 2.0. Both of Fig. 8a and b exhibit that the overall strength is decreased with the increasing thickness, and the variation gradient of the normalized peak load decreases with the increasing thickness. Nevertheless, substantial discrepancy has been found between the two figures. Considering the category of $\eta = 1.0$, the variation of the normalized peak load for $\sigma_f/\sigma_s = 1.0$ is remarkable, while that for $\sigma_f/\sigma_s = 2.0$ is very slight. In other words, the difference between the cases for large and small values of σ_f/σ_s is sharp. However, the situation is significantly different considering the category of $\eta = 10$ shown in Fig. 8b. The difference between the cases for $\sigma_f/\sigma_s = 1.0$ and $\sigma_f/\sigma_s = 2.0$ can be still observed, but not so noticeable as the category of $\eta = 1.0$.

As pointed out by aforementioned text, the strength ratio σ_f/σ_s could be regarded as the parameter to assess the strain hardening capacity of adhesives which is stronger for a higher value of σ_f/σ_s . Generally, the strain hardening capacity of adhesives is independent of their toughness that is related to the energy absorption capacity of adhesive during the fracture process of adhesives, while the strain hardening is related to the deformation-resistance capacity after the yield strength is reached. In fact, some ductile adhesives appear strong strain hardening capacity (e.g., Hysol EA 9321, Loctite) whilst the other ductile adhesives

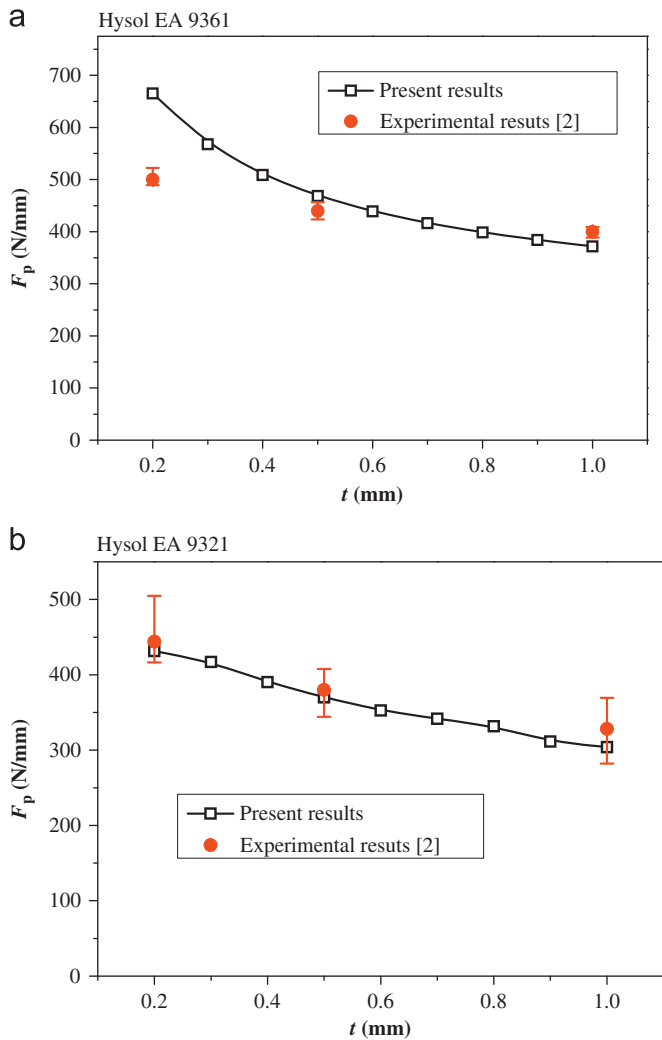


Fig. 5. Peak load plotted as a function of adhesive thickness for (a) Hysol EA 9361 and (b) Hysol EA 9321; comparison between the present model predictions with the experimental results [2].

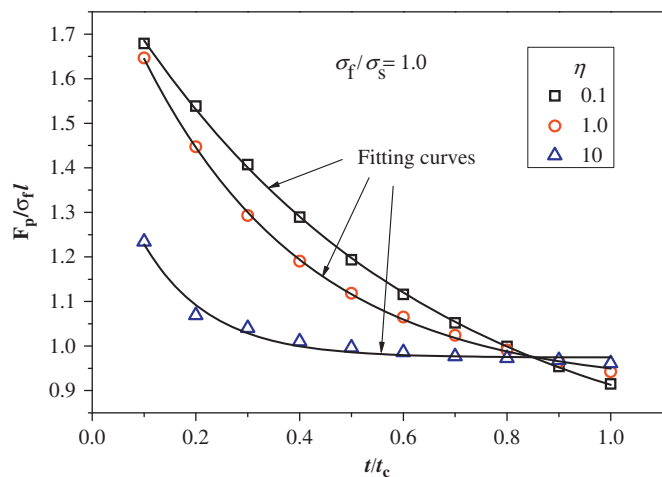


Fig. 6. Influence of selected toughness ratios η on the relationship between the peak load and the adhesive thickness.

appear weak strain hardening (e.g., Hysol EA 9359.3, Loctite), depending on their types. Similar examples would be also found among the brittle adhesives.

Table 2
Values of fitting parameters for Eq. (26).

η	A_1	A_2	A_3
0.1	1.16649	0.58297	0.70311
1.0	1.01137	0.31844	0.90587
10	0.54733	0.13000	0.97430

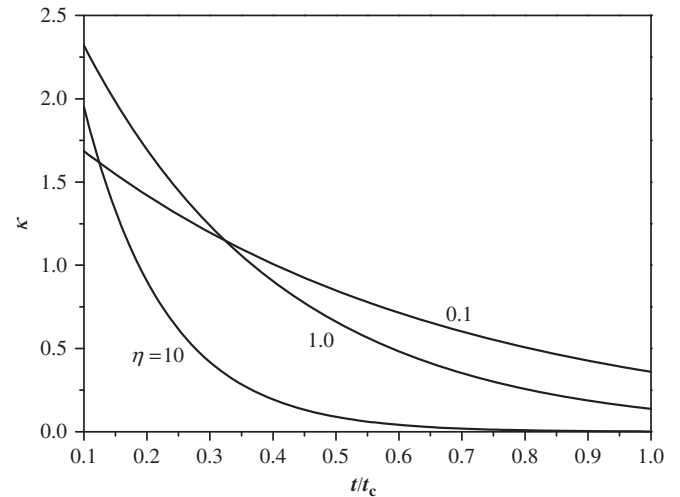


Fig. 7. Gradient of the variation in peak load κ plotted as a function of adhesive thickness for the selected toughness ratios η .

Based on the observation from Fig. 8 considering the combined influence of σ_f/σ_s and η , it is concluded that variation of overall strength corresponding to weak hardening adhesive is more remarkable compared to that corresponding to strong hardening adhesive, especially for the brittle adhesive in the comparatively small thickness range.

4.4. Further discussion

It is worth mentioning that, in the present research, some issues are still not resolved and should be considered in future.

Firstly, the adherends for the present model are high strength steel with high yield strength and Young's modulus, the deformation of the adherends is hence slight and there is almost no plasticity in them. Accordingly, the small-scale yield assumptions are approximately satisfied in the present model. Noting that the estimate approach of cohesive parameters in Section 3 is applicable only under the small-scale yield assumptions, thus considering other metallic adherends susceptible to plastic deformation and the corresponding estimate approach for thickness-dependence cohesive parameters are needed in the future work.

Secondly, the failure mode of the joint is another key issue. In fact, depending on the loading and boundary conditions, for the metallic bonded joints, there may be two different failure modes: (a) adhesion failure occurring at the interfacial surface between the adherends and the adhesive layer and (b) cohesion failure occurring in the adhesive layer [36]. However, in the present model, only the cohesion failure with the underlying crack path in the middle of the adhesive layer is carried out and the other failure mode is not taken into account. It is anticipated that the two different failure modes would involve different plastic zone sizes and different magnitudes of the plastic strains. Therefore, the situations for other failure mode and crack path should be further investigated.

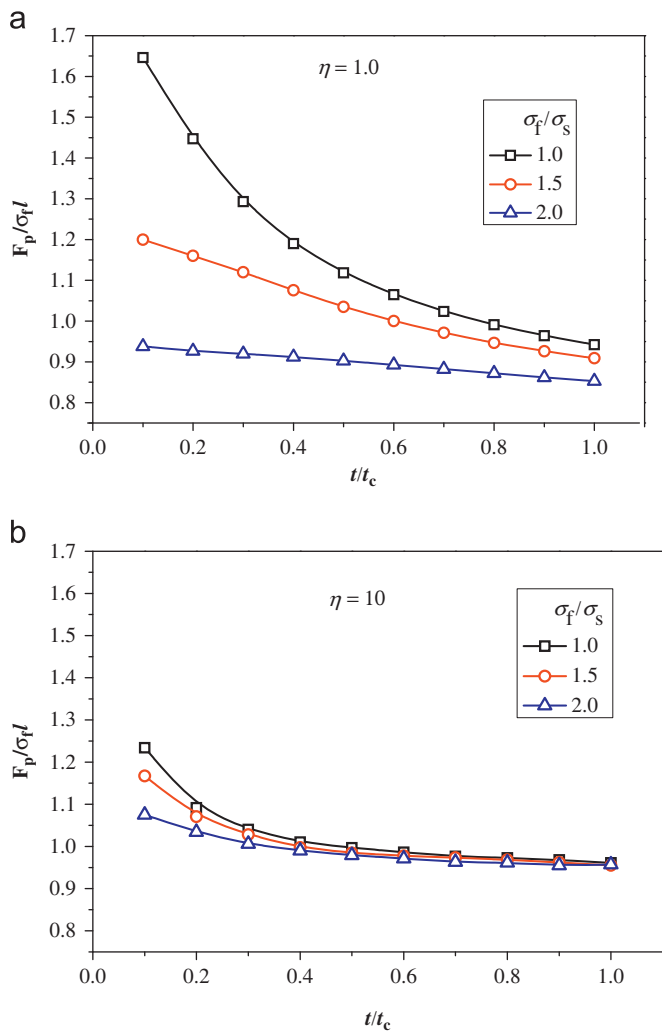


Fig. 8. Influence of selected strength ratios σ_f/σ_s on the relationship between the peak load and the adhesive thickness, with an identical toughness ratio: (a) $\eta = 1.0$ and (b) $\eta = 10$.

Finally, in practice, the amounts of defects such as micro-voids and micro-cracks are larger in thicker adhesive layers, reducing the bonding capacity accordingly [32], whereas the present model does not consider the influence of the defects, just considering the cohesive parameters affected by the adhesive thickness. More sophisticated models are needed to study the combined effect of both the adhesive thickness and defects.

5. Conclusions

In summary, the influence of the adhesive thickness on both the cohesive parameters and overall strength of metallic adhesive bonding structures are investigated, with the CZM employed to simulate the adhesive layers with a series of thicknesses. A theoretical approach has been developed to determine the CZM parameters for the present model when the adhesive thickness is varied. And then some numerical examples are given to display the thickness-dependence overall strength of the adhesive joints, followed by some comparisons with the existing experimental results. Furthermore, the variations of the cohesive parameters and the overall strength with the various thicknesses are affected by some factors relating to the toughness and strain hardening capacity of adhesives, which are investigated finally. The results

show that both the cohesive parameters and the overall strength of metallic adhesive bonding structures are much dependent on the adhesive thickness. Moreover, as the thickness is varied, the variation of overall strength corresponding to weak hardening adhesive is more remarkable compared to that corresponding to strong hardening adhesive, especially for the brittle adhesive in the comparatively small thickness range.

Acknowledgments

This work was supported by the National Natural Science Foundation of China (11021262, 10932011, and 91116003), by National Basic Research Program of China through 2012CB937500.

Appendix: A

In Section 4.1, the peak loads are obtained for the underlying load–displacement relations of SLJ subjected to the tensile loading. Fig. A1 shows the typical load–displacement curves of SLJ with the two types of adhesives having the thickness of 1.0 mm.

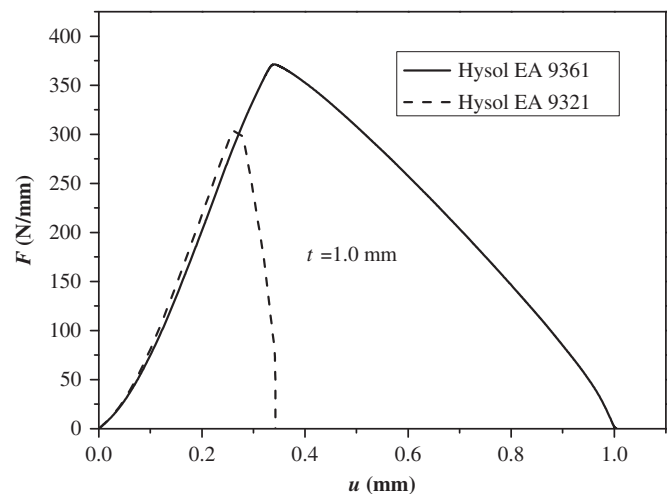


Fig. A1. Typical load–displacement curves of SLJ with two types of adhesives.

References

- [1] da Silva LFM, Crichtlow GW, Figueiredo MAV. Parametric study of adhesively bonded single lap joints by the Taguchi method. *J Adhes Sci Technol* 2008;22:1477–94.
- [2] da Silva LFM, Rodrigues TNSS, Figueiredo MAV, de Moura MFSF, Chousal JAG. Effect of adhesive type and thickness on the lap shear strength. *J Adhes* 2006;82:1091–115.
- [3] Kahraman R, Sunar M, Yilbas B. Influence of adhesive thickness and filler content on the mechanical performance of aluminum single-lap joints bonded with aluminum powder filled epoxy adhesive. *J Mater Process Technol* 2008;205:183–9.
- [4] Castagnetti D, Spaggiari A, Dragoni E. Effect of bondline thickness on the static strength of structural adhesives under nearly-homogeneous shear stresses. *J Adhes* 2011;87:780–803.
- [5] Chai H. The effects of bond thickness, rate and temperature on the deformation and fracture of structural adhesives under shear loading. *Int J Fract* 2004;130:497–515.
- [6] Lee DB, Ikeda T, Miyazaki N, Choi NS. Effect of bond thickness on fracture toughness of adhesive joints. *J Eng Mater Technol* 2004;126:14–8.
- [7] Goglio L, Rossetto M. Stress intensity factor in bonded joints: influence of the geometry. *Int J Adhes Adhes* 2010;30:313–21.
- [8] Goglio L, Rossetto M, Dragoni E. Design of adhesive joints based on peak elastic stresses. *Int J Adhes Adhes* 2008;28:427–35.

- [9] Yan C, Mai YW, Yuan Q, Ye L, Sun J. Effects of substrate materials on fracture toughness measurement in adhesive joints. *Int J Mech Sci* 2001;43:2091–102.
- [10] Marzi S, Biel A, Stigh U. On experimental methods to investigate the effect of layer thickness on the fracture behavior of adhesively bonded joints. *Int J Adhes Adhes* 2011;31:840–50.
- [11] Pardoën T, Ferracin T, Landis CM, Delannay F. Constraint effects in adhesive joint fracture. *J Mech Phys Solids* 2005;53:1951–83.
- [12] Azari S, Papini M, Spelt JK. Effect of adhesive thickness on fatigue and fracture of toughened epoxy joints—part II: analysis and finite element modeling. *Eng Fract Mech* 2011;78:138–52.
- [13] Azari S, Papini M, Spelt JK. Effect of adhesive thickness on fatigue and fracture of toughened epoxy joints—part I: experiments. *Eng Fract Mech* 2011;78:153–62.
- [14] Ikeda T, Yamashita A, Lee D, Miyazaki M. Failure of a ductile adhesive layer constrained by hard adherends. *J Eng Mater Technol* 2000;122:80–5.
- [15] Kinloch AJ, Shaw SJ. The fracture-resistance of a toughened epoxy adhesive. *J Adhes* 1981;12:59–77.
- [16] Duan K, Hu XZ, Mai YW. Substrate constraint and adhesive thickness effects on fracture toughness of adhesive joints. *J Adhes Sci Technol* 2004;18:39–53.
- [17] Daghyani HR, Ye L, Mai YW. Mode-I fracture behaviour of adhesive joints. 1. Relationship between fracture energy and bond thickness. *J Adhes* 1995; 53:149–62.
- [18] Ji GF, Ouyang ZY, Li GQ. On the interfacial constitutive laws of mixed mode fracture with various adhesive thicknesses. *Mech Mater* 2012;47:24–32.
- [19] Ji GF, Ouyang ZY, Li GQ. Effects of bondline thickness on mode-II interfacial laws of bonded laminated composite plate. *Int J Fract* 2011;168:197–207.
- [20] Ji GF, Ouyang ZY, Li GQ, Ibekwe S, Pang SS. Effects of adhesive thickness on global and local mode-I interfacial fracture of bonded joints. *Int J Solids Struct* 2010;47:2445–58.
- [21] Carlberger T, Stigh U. Influence of layer thickness on cohesive properties of an epoxy-based adhesive—an experimental study. *J Adhes* 2010;86:814–33.
- [22] Chandra N, Li H, Shet C, Ghonem H. Some issues in the application of cohesive zone models for metal–ceramic interfaces. *Int J Solids Struct* 2002;39:2827–55.
- [23] Camanho PP, Davila CG, de Moura MF. Numerical simulation of mixed-mode progressive delamination in composite materials. *J Compos Mater* 2003;37:1415–38.
- [24] Balzani C, Wagner W. An interface element for the simulation of delamination in unidirectional fiber-reinforced composite laminates. *Eng Fract Mech* 2008;75:2597–615.
- [25] de Moura MFSF, Campilho RDSG, Goncalves JPM. mixed-mode cohesive damage model applied to the simulation of the mechanical behaviour of laminated composite adhesive joints. *J Adhes Sci Technol* 2009;23:1477–91.
- [26] Lee MJ, Cho TM, Kim WS, Lee BC, Lee JJ. Determination of cohesive parameters for a mixed-mode cohesive zone model. *Int J Adhes Adhes* 2010;30:322–8.
- [27] Högberg JL. Mixed mode cohesive law. *Int J Fract* 2006;141:549–59.
- [28] Gustafson PA, Waas AM. The influence of adhesive constitutive parameters in cohesive zone finite element models of adhesively bonded joints. *Int J Solids Struct* 2009;46:2201–15.
- [29] Wei Y, Zhao HF. Peeling experiments of ductile thin films along ceramic substrates—critical assessment of analytical models. *Int J Solids Struct* 2008;45:3779–92.
- [30] Wei Y, Hutchinson JW. Models of interface separation accompanied by plastic dissipation at multiple scales. *Int J Fract* 1999;95:1–17.
- [31] Zhuk AV, Evans AG, Hutchinson JW, Whitesides GM. The adhesion energy between polymer thin films and self-assembled monolayers. *J Mater Res* 1998;13:3555–64.
- [32] Xu W, Wei Y. Strength analysis of metallic bonded joints containing defects. *Comput Mater Sci* 2012;53:444–50.
- [33] Yang QD, Thouless MD. Mixed-mode fracture analyses of plastically-deforming adhesive joints. *Int J Fract* 2001;110:175–87.
- [34] da Silva LFM, Carbas RJC, Critchlow GW, Figueiredo MAV, Brown K. Effect of material, geometry, surface treatment and environment on the shear strength of single lap joints. *Int J Adhes Adhes* 2009;29:621–32.
- [35] de Moraes AB, Pereira AB, Teixeira JP, Cavaleiro NC. Strength of epoxy adhesive-bonded stainless-steel joints. *Int J Adhes Adhes* 2007;27:679–86.
- [36] Xu W, Wei Y. Strength and interface failure mechanism of adhesive joints. *Int J Adhes Adhes* 2012;34:80–92.